# Frequency-Agile Beam-Switchable Antenna

Chao Gu, Steven Gao, *Senior Member, IEEE*, Benito Sanz-Izquierdo,
Edward A. Parker, Wenting Li, Xuexia Yang, and Zhiqun Cheng

***Abstract*— A novel antenna with both frequency and pattern reconfigurability is presented. The reconfigurability is achieved by integrating an active frequency selective surface (AFSS) with feed antenna. The smart FSS comprises a printed slot array loaded by varactors. A novel dc biasing arrangement is proposed to feed the slots vertically so that the unwanted effects caused by bias lines are minimized. A monopole antenna is designed to illuminate the AFSS. The resulting structure can operate in a frequency tuning range of 30%. By reconfiguring the different sections of active FSS cylinder into a transparent or reflector mode, the omnidirectional pattern of the source antenna can be converted to a directive beam. As an illustration, half of the AFSS cylinder is successively biased, enabling the beam switching to cover the entire horizontal plane over a range of frequencies. An antenna prototype was fabricated and measured. Experimental results demonstrate the capability of providing useful gain levels and good impedance matching from 1.7 to 2.3 GHz. The antenna offers a low-cost, low-power solution for wireless systems that require frequency and beam reconfigurable antennas. The proposed design consumes about 1000 times less dc power than the equivalent narrowband beam-switching antenna design using p-i-n diode-loaded AFSS.**

***Index Terms*— Beam steering, frequency and beam reconfigurable, frequency selective surface (FSS), frequency tunable, reconfigurable antennas.**

## I. Introduction

FUTURE wireless networks are going to evolve to provide significant improvements, such as higher data rates, reduced end-to-end latency, and lower power consumption. Most wireless systems employ multiple antennas, which can lead to increased hardware complexity, large size, high power consumption, and high cost [1]. Reconfigurable antennas [2]–[6], with the capacity to electronically alter their operating modes, have been extensively studied during the past few decades. Such reconfigurable antennas are important for achieving optimum performance of wireless systems under various environmental conditions. Compared with frequency-switched antennas, which operate at some predefined separate frequency bands [7], [8], frequency-tunable antennas can achieve dynamic control of relatively narrow instantaneous bandwidths, and thus allowing operation over a larger bandwidth. Various continuous frequency tuning techniques employing varactors can be found in the literature [9]–[13]. A dual-band reconfigurable slot antenna is presented in [11], where two varactors are placed in appropriate locations of the slot to achieve dual-frequency operation. Hum and Xiong [12] propose a differentially fed, frequency agile patch antenna incorporating three pairs of varactors. The tuning range for −10-dB reflection coefficient is approximately from 1.8 to 3.15 GHz. Reference [13] presents a coplanar waveguide wideband monopole antenna integrated with a frequency tunable bandpass filter. The resulting antenna is demonstrated to have a tuning range from 2.88 to 4.62 GHz and a 50% gain reduction at the higher frequencies. Despite continuous frequency tuning, the beams of the reported antennas in [9]–[13] are all fixed.

Pattern reconfigurable antennas, on the other hand, can be exploited as a cost-effective substitute for conventional phased arrays that consist of expensive RF components, such as phase shifters and amplifiers. By subtly steering the antenna main beam toward the intended users, a pattern reconfigurable antenna can be used to suppress multipath fading and increase channel capacity. Much work has been done to design low-cost, pattern reconfigurable antennas incorporating RF switches [14], [15]. However, there are few solutions available for combining both frequency and pattern reconfigurability into a single antenna structure. A frequency-agile, switched-beam antenna array described in [16] is capable of switching four beams using switched line phase shifters. But the antenna can only operate at two fixed frequencies (4.7 and 7.5 GHz). The combination of frequency and pattern reconfigurability into the same antenna leads to a simplified and highly integrated solution for size-constrained multifunction platforms where diversity schemes are employed to improve the system performance, for example, in multiple-input multiple-output communication systems.

More recently, metamaterials and periodic structures have been applied to reconfigure radiators [17]–[20]. By integrating tunable surfaces [21]–[25] with conventional antennas, it is feasible to develop antennas with multireconfigurability [9]. Costa *et al.* [26] present a frequency tunable and beam steerable antenna consists of a wideband bow-tie radiating element over an active artificial magnetic conductor. The measured results show a −10-dB $S_{11}$ tuning range from 2.3–3.0 GHz (26.4%) with broadside beam steering. The antenna has a low profile but its beam cannot steer over the entire horizontal plane. Electronic beam-switching antennas employing active frequency selective surface (FSS) have been an active research area in the last decade due to their potential

Manuscript received September 24, 2016; revised January 24, 2017; accepted April 15, 2017. Date of publication June 16, 2017; date of current version August 2, 2017. This work was supported by the EPSRC under Grant EP/N032497/1. *(Corresponding author: Chao Gu.)*

C. Gu, S. Gao, B. Sanz-Izquierdo, E. A. Parker, and W. Li are with the School of Engineering and Digital Arts, University of Kent, Canterbury CT2 7NT, U.K. (e-mail: s.gao@kent.ac.uk).

X. Yang is with the School of Communication Engineering, Shanghai University, Shanghai 200444, China.

Z. Cheng is with the School of Electronic Engineering, Hangzhou Dianzi University, Hangzhou 310018, China.

Color versions of one or more of the figures in this paper are available online at http://ieeexplore.ieee.org.

Digital Object Identifier 10.1109/TAP.2017.2713978

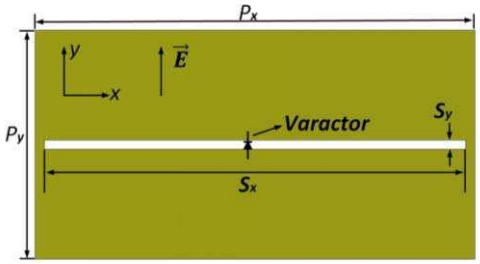


Fig. 1. Schematic of the ideal all-metal unit cell.

of achieving multireconfigurability. Unfortunately, the narrow impedance matching and radiation bandwidth of the published work [27]–[30] hinder their applications in practical systems.

In this paper, a novel frequency-tunable and beam-switchable antenna comprising a tunable FSS fed by a monocone antenna is presented. In contrast to the previously reported active FSS-based antennas [27]–[30], this paper uses varactor diodes instead of switching diodes. The use of varactor diodes enables the continuous tuning of antenna operating frequency in a wide frequency range. It is also viable to achieve beam switching at any frequency within the tuning range. More importantly, it consumes a tiny fraction of the dc power required to achieve all this. This paper is organized as follows. Section II discusses the novel biasing arrangement and how the active FSS is optimized. Section III describes the source antenna employed and analyses the effect of the metallic reflector as the reference antenna. Section IV presents the fabrication and measurements results. Finally, Section V discusses the results and the benefits of this paper, and Section VI provides some conclusions.

## II. Active FSS Design

Various FSS tuning applications can be found in the literature [21]–[24], but most of them cannot be applied to design beam switching antennas. Based on the previous work [30], it is feasible to employ the biasing technique comprising a double-sided structure where bias lines can be hidden behind the passive FSS. The whole structure is easy to be fabricated and no metallic through via is needed. Also, a thin flexible substrate is chosen in order to easily reshape the planar active FSS (AFSS) into a cylindrical one. The biasing structure, however, needs careful design to minimize potential unwanted resonances.

### A. Ideal FSS Unit Cell Analysis and Modeling

As a preliminary examination of the tunability of the slot FSS, an ideal all-metal unit cell is simulated using the Floquet mode of the frequency domain solver in CST. The metal-only FSS unit cell consists of a half-wavelength slot in the center of a copper plate, as shown in Fig. 1. A varactor is connected between the gap and the physical bias circuit is excluded for simplicity. The dimensions of the unit cell in Fig. 1 are $P_x = 48$ mm, $P_y = 25$ mm, $S_x = 46$ mm, and $S_y = 0.2$ mm. The slot FSS is a relatively simple structure, which makes it a good option for AFSS design as it comparatively lowers the complexity of the biasing circuit.

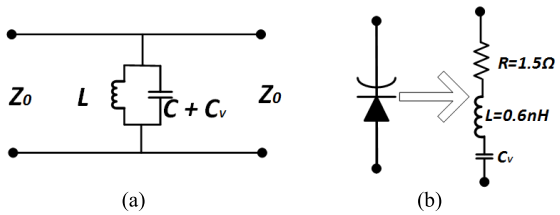


Fig. 2. EC model of (a) tunable unit cell and (b) varactor.

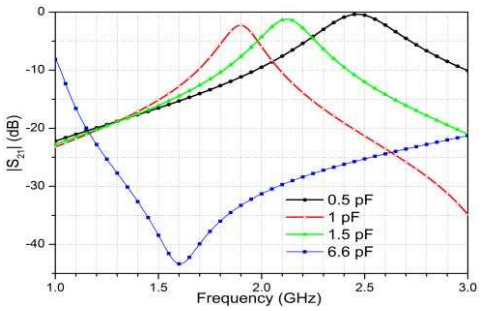


Fig. 3. Simulated transmission coefficients of the ideal unit cell.

To fully understand the tuning mechanism of the FSS, an equivalent circuit (EC) model is used as a simpler and faster method than full-wave simulation in CST. Fig. 2(a) shows the EC model derived from transmission line analogy. Essentially, the EC model is simply a parallel *LC* circuit. The inductance is associated with the electric current flowing in the patch and the capacitance consists of an intrinsic capacitance $C$ between the gap of the slot and the variable capacitance $C_v$ from the varactor diode. According to the bandpass filter theory, the resonance frequency of the FSS can be expressed as follows:

$$f = 1/[2\pi\sqrt{L(C + Cv)}]. \quad (1)$$

It is clear that from (1), increasing the capacitance of the varactor shifts the resonance frequency downward. The tuning range is limited by the capacitance ratio of the varactor. Normally, higher ratios yield wider frequency tuning ranges. Here, we used an Infineon BB857 silicon varactor whose capacitance tunable range is from 0.52 to 6.6 pF. To simplify the simulation, the varactor is modeled as a series *RLC* circuit with a series inductance of 0.6 nH and resistance of 1.5 Ω, as shown in Fig. 2(b). Fig. 3 shows the simulated transmission coefficients of the ideal slot FSS without bias network for different capacitance values. It can be noted that by varying the capacitance from 0.5 to 1.5 pF, the slot resonance frequency can be tuned from 2.5 to 1.9 GHz with an acceptable transmission level. More importantly, the curve for 6.6 pF shows that between 1.2 and 3 GHz, the $S_{21}$ level is below −20 dB, which means almost no EM wave can be transmitted through the FSS. This is an extremely good feature for reconfiguring the FSS as a reflector, which is explored for the eventual structure.

### B. Bias Network Design

The bias network is the most critical part of the active FSS design. Maintaining a simple network is beneficial for minimizing the unwanted effect caused by the bias lines. In our

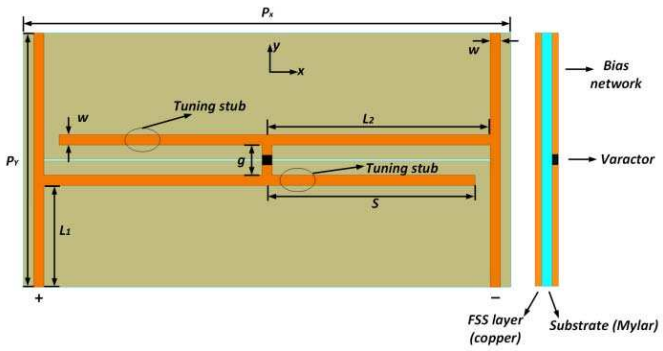


Fig. 4. Schematic of the resulting bias network.

TABLE I
BIAS NETWORK DIMENSIONS [mm]

| $L_1$ | $L_2$ | $w$ | $g$ | $S$ | $P_x$ | $P_y$ |
|---|---|---|---|---|---|---|
| 10.5 | 22.5 | 1 | 2 | 20.5 | 48 | 25 |

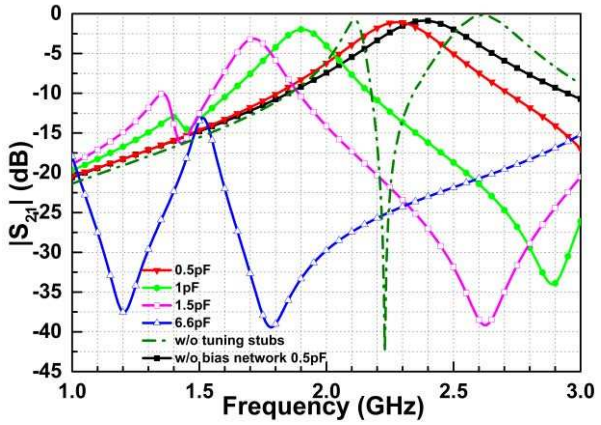


Fig. 5. Simulated transmission coefficients of the unit cell with bias network.

design, it is preferred that all the varactors are parallel fed to limit the maximum control voltage. Fig. 4 shows the devised network, which is etched on the other side of the substrate. Here, 0.05-mm-thick Mylar film with $\varepsilon_r = 2.7$ and loss tangent of 0.0023 is used as it is flexible and can be used for conformal antenna applications. As can be seen from Fig. 4, two dc main control lines are located at each side of the slot, providing positive and negative connections for the varactor. The package size of the diode is about 2 mm×1 mm so the gap between the two pads for bridging the varactor is 2 mm and the width of the bias line are set to be 1 mm. The dimensions of the bias network are given in Table I. Fig. 5 shows the simulated transmission coefficients of the entire unit cell consisting of the substrate and bias lines.

The black line denotes the $S_{21}$ of the unit cell with the substrate but excluding the bias lines at $C_v = 0.5$ pF. Compared with the corresponding one in Fig. 3, adding a thin substrate has shifted the resonance frequency by 70 MHz, which is a minor effect. The other curves for different capacitances show that the transmission losses increase by adding the bias network. There are multiple resonances at lower frequencies, but they have no effect on the tunable range of

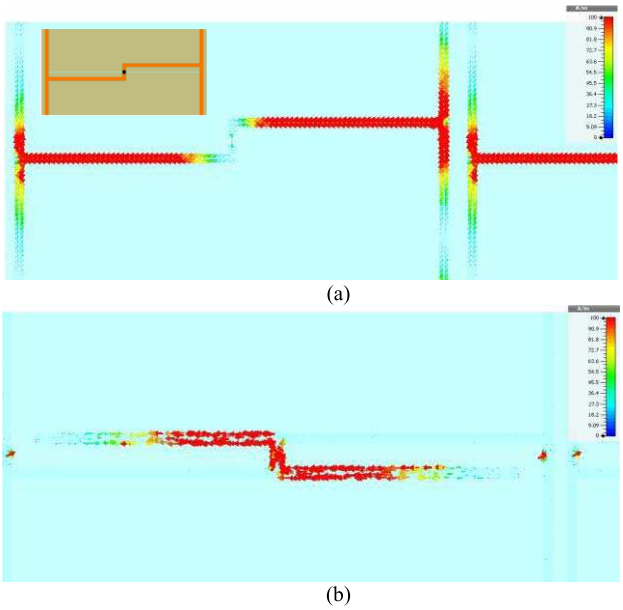


Fig. 6. Simulated current distributions on bias network at 2.4 GHz. (a) Without tuning stubs. (b) With tuning stubs.

the AFSS. It is worth noting that when the varactor is tuned to 6.6 pF, the whole surface acts like a reflector, blocking signals from 1.5 to 3.0 GHz.

### C. Tuning Stub Effect

In active FSS designs, the bias network, if not well designed, will impact upon the frequency response of the entire resonant surface. In some cases, with the bias lines etched on the other side of the substrate, the frequency response of the FSS deteriorates when the network is complex and comparable to the wavelength. Indeed, the structure can be treated as a bandpass FSS layer (i.e., the slots) cascading a band-stop patch-type FSS (i.e., the bias lines), as the incident wave excites the bias network especially when the AFSS is close to an antenna feed. Thus, in this paper, two tuning stubs are used to maintain the desired transmission responses. The simulated current distribution at 2.4 GHz for the two cases is shown in Fig. 6. It is clear that without the tuning stubs, the induced currents are mostly along the bias lines and partially on the two vertical lines. This can be detrimental to the transmission coefficients as can be seen from Fig. 5 (dotted line). There is a band-stop pole from 2.2 to 2.4 GHz, which is exactly at the desired working frequencies. It can be noted from Fig. 6(b) that with the tuning stubs, the induced currents concentrate on the half tuning stubs only. There is negligible current distributed on the vertical lines. In light of the aforementioned discussion, the two stubs provide a method to detune the resonating bias network, enabling a reduction of the circuit resonance frequency and thus mitigating the effect caused by the network.

## III. FREQUENCY TUNABLE ANTENNA DESIGN

After the investigation of the planar active FSS, the next step is to integrate it with a feed antenna. The planar FSS is rolled into a cylinder to mimic a corner reflector antenna.

TABLE II
METALLIC REFLECTOR ANTENNA DIMENSIONS [mm]

| $D$ | $h_1$ | $h_2$ | $G$ | $t$ | $R_g$ | $R_c$ | $H$ |
|---|---|---|---|---|---|---|---|
| 37 | 50 | 40 | 2 | 0.5 | 74 | 76 | 200 |

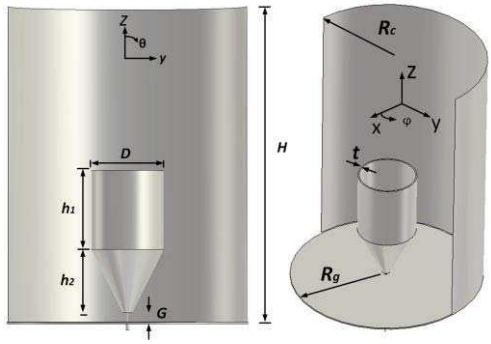


Fig. 7. Schematic of the metallic reflector antenna.

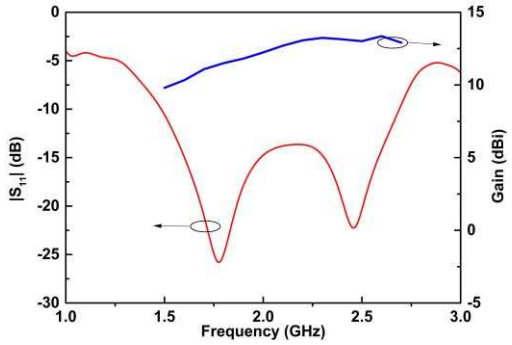


Fig. 8. Simulated reflection coefficient and gain of the reference antenna.

### A. Metallic Reflector Antenna

It is necessary to investigate the reflector antenna to give some design guidance about the influence of AFSS size, feeder dimensions, and so on. A conical monopole antenna is used as the radiator, as shown in Fig. 7. The dimensions of the reflector antenna are given in Table II.

The metallic reflector antenna is used as a reference and optimized to have stable performance in terms of impedance matching and gain. Fig. 8 shows the simulated reflection coefficient and gain of the antenna. The operating frequency covers 1.5–2.7 GHz. It can be noted that the gain rises gradually owing to the increased aperture size. The computed radiation patterns are shown in Fig. 9.

### B. AFSS Antenna Design

The parameters of the reference antenna, $R_c$ and $H$ (Table II), can be used as the initial values for the active FSS cylinder design. Before rolling the planar FSS into a cylinder, the number of unit cells along the circumference and axis is deduced from the following equations:

$$N_x = 2\pi \times R_c / P_x \tag{2}$$

$$N_y = H / P_y. \tag{3}$$

The final structure consisted of 10 columns and 8 rows, as shown in Fig. 10. Note that a half cylindrical AFSS and

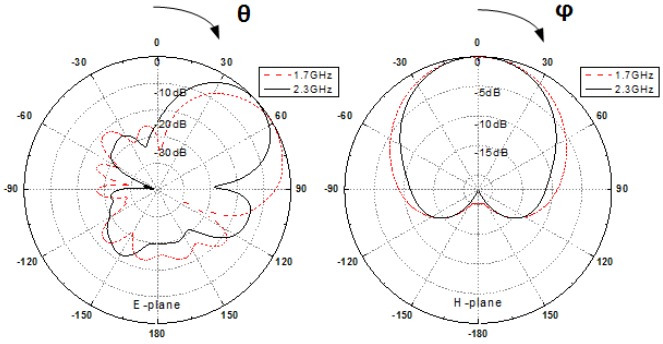


Fig. 9. Simulated radiation patterns of the reference antenna.

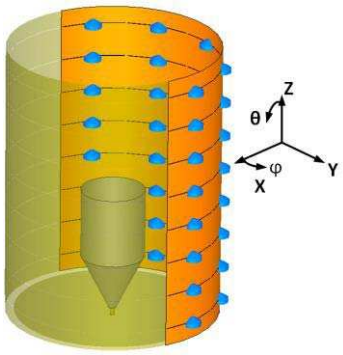


Fig. 10. Schematic of the final antenna structure.

diodes have been made transparent in Fig. 10 for clarity. The dimensions of the resulting antenna are the same as those of the metallic reflector antenna except that the reflector is replaced by the cylindrical AFSS. To explore the feasibility of the frequency tuning and beam switching, the entire configuration is simulated CST using the frequency-domain solver. To avoid generating excessively large numbers of meshcells and to reduce the computing time, the thin substrate and the bias network are not included in the simulation, and the numerical results are nevertheless a reliable guide in evaluating the experiment results. To demonstrate the frequency tunability of the antenna, a series of capacitance values of the varactor is chosen in order to obtain different $S_{11}$ ranges. All the values are extracted from the data sheet provided by the manufacturer.

Fig. 11 compares the simulated $S_{11}$ of the antenna in various states. The yellow area denotes the operational frequency range. It can be seen that the usable frequency band can be shifted upward as the capacitance decreases gradually. There are multiple reflections inside the cylinder, resulting in corresponding resonance frequencies. But at those irrelevant frequencies, the antenna is inefficient, since the aperture of the AFSS is only optimized for the specified band. Fig. 12 shows the radiation patterns at different capacitances. It is clear that the tilt angle in the E-plane increases when increasing the resonance frequency, whereas the beamwidth in the H-plane decreases. The backlobe levels are all below $-15$ dB. The simulated gains at the various states are shown in Fig. 13. It can be noted that the peak gain can be tuned with the same trend as with the metallic reflector antenna. Meanwhile, the gain at each state has a certain bandwidth. Therefore,

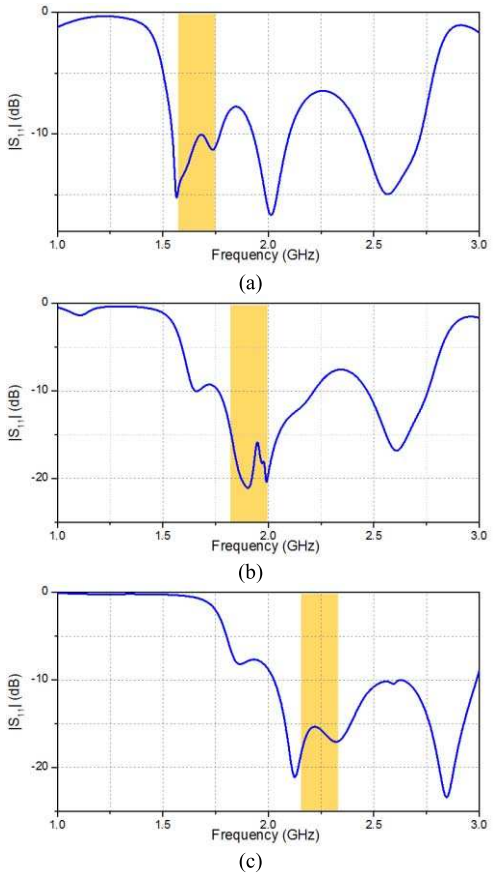


Fig. 11. Simulated $S_{11}$ of the antenna at (a) 1.5, (b) 1, and (c) 0.5 pF.

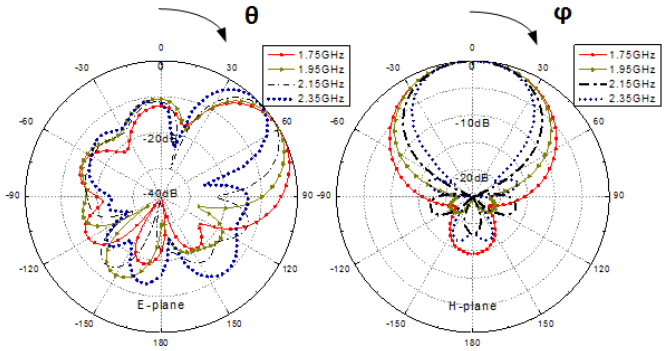


Fig. 12. Simulated radiation patterns at specific frequencies.

by gradually increasing the bias voltage applied to the varactors, the peak gain value increases with frequency for each bias voltage. Fig. 14 shows simulated five beam-switching states for the diode capacitance 1 pF (corresponding to the resonance frequency of 1.95 GHz) in the H-plane. If five columns are successively reconfigured as a reflector, in total ten beams can be generated to cover the horizontal plane.

## IV. Antenna Fabrication and Measurement

To verify the simulated planar FSS, a prototype was fabricated and measured in a plane wave chamber. A photograph of the AFSS and resulting antenna under test is shown in Fig. 15. The measured transmission response of the tunable FSS at

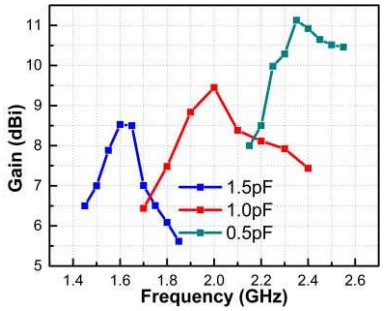


Fig. 13. Simulated gain ranges at different diode states.

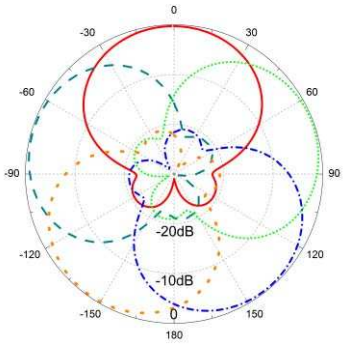


Fig. 14. Simulated switched beams at 1 pF in the H-plane.

Fig. 15. Fabricated bias circuit on the substrate and the final antenna.

different dc voltages is shown in Fig. 16. As can be seen from Fig. 16, the resonance frequency increased from 1.75 GHz for 7.6 V to 2.35 GHz for 28.1 V, while the passband insertion loss reduced from 3 to 0.5 dB. Moreover, when the capacitance is tuned to 6.6 pF at 0 V, the FSS is switched to reflection mode as the transmission coefficients are all below −12 dB across the tuning range. This feature is favorable for the beam switching antenna design as it requires zero control power.

A polystyrene foam is used to support the FSS cylinder above the ground plane. The dc control lines can be hidden under the metal ground plane of the monocone antenna, shielding the unwanted signal from the cables. As discussed in Section III-B, half of the AFSS cylinder is required to be applied a variable voltage, while the other half is left with zero bias voltage. Fig. 17 shows the details of the bias network. To simplify the dc control system, all the positive lines are combined together and connected to the positive of the power supply, which has a tuning range of 0–30 V, and hence switching ON/OFF the negative lines can control each column of the AFSS cylinder. Moreover, to activate a half cylinder, five negative lines can be connected to the negative

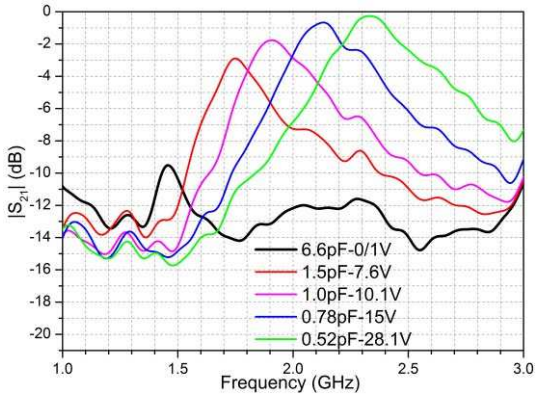


Fig. 16. Measured transmission coefficients of the tunable FSS.

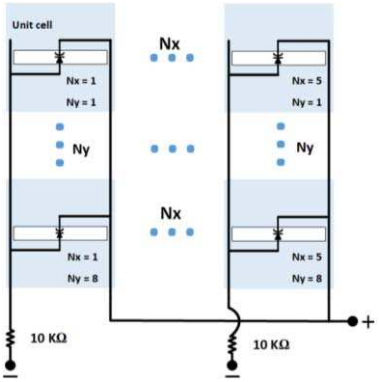


Fig. 17. Schematic of the bias network of half AFSS.

of the power supply. When integrated into a larger system, the positive line here could become the common ground, while the structure would be controlled through varying negative voltages. Nevertheless, the flexibility of the biasing configuration allows the use of a common ground on the negative lines and varying positive voltages. It should be noted that the 10-k$\Omega$ resistors are only used for protection and isolation purposes. Fig. 18 compares the measured reflection coefficients versus frequency at the corresponding bias voltages. It is noted that the antenna impedance matching ranges can be tuned with the applied voltage. Theoretically, the poles of $S_{11}$ are in accordance with the resonance frequencies of the AFSS transmission coefficients. Note that there is a slight frequency shift at most of the bias voltages and a 150-MHz discrepancy at 28.1 V. Still, the antenna remains well matched at each range of the operating frequency.

Following the validation of the $S$-parameters, the antenna was measured in an anechoic chamber. Fig. 19 shows the measured gains for the four bias voltages. As predicted, the peak gain is tuned from 1.7 to 2.3 GHz, which corresponds to a 30% range. Compared with the simulated gains in Fig. 13, the tunable range is slightly smaller than the simulated results from 1.65 to 2.3 GHz. Note that this range is close to the one of the measured passband in Fig. 16. There is a good reason to believe that the FSS can be regarded as a spatial filter and when it is integrated with an antenna, the gain tunability of the resulting antenna follows the same trend of the passband tunability of the filter. As can be seen from Figs. 13 and 19,

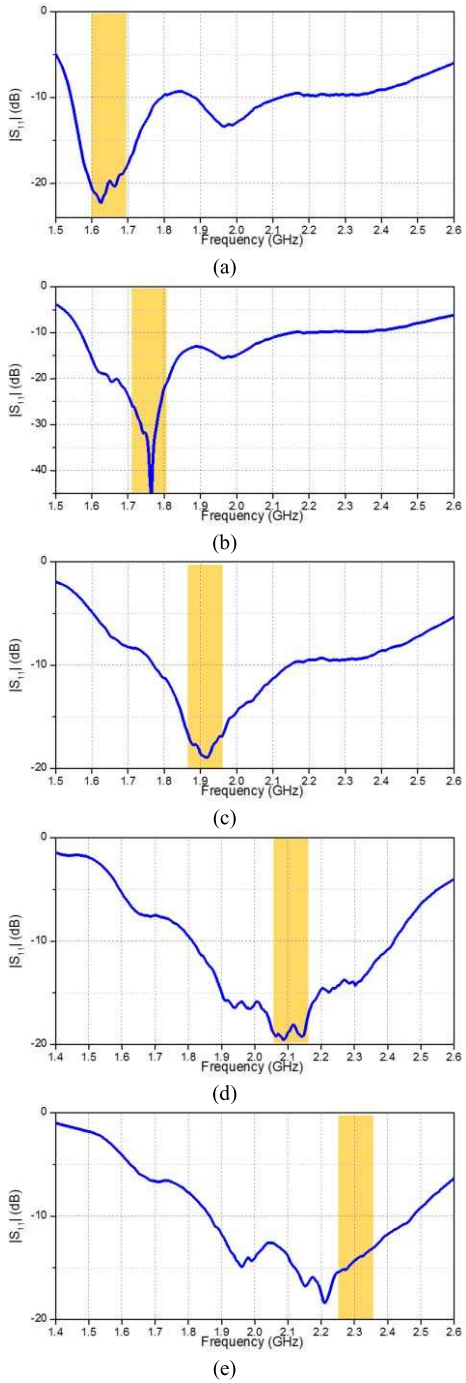


Fig. 18. Measured antenna reflection coefficients at (a) 7, (b) 8, (c) 10.1, (d) 15, and (e) 28.1 V.

there is a measured gain drop of 2.5 dB, and a simulated gain drop of 3 dB. This antenna gain drop occurs for the following two main reasons. First, since the frequency tuning range is from 1.6 to 2.4 GHz, the effective aperture size is smaller at the lower frequencies. The gain of the aperture antenna decreases with frequency. Second, as can be seen from Fig. 16, the active FSS is designed and optimized at around 2.4 GHz, and the transmission coefficient drops when tuning the FSS from 2.4 GHz to the lower frequencies. The reflected waves cause multiple reflections and feed blockage inside the antenna structure, and thus, the antenna efficiency

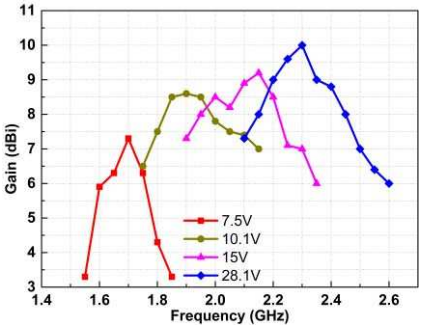


Fig. 19. Measured antenna gain tuning ranges for the four bias voltages.

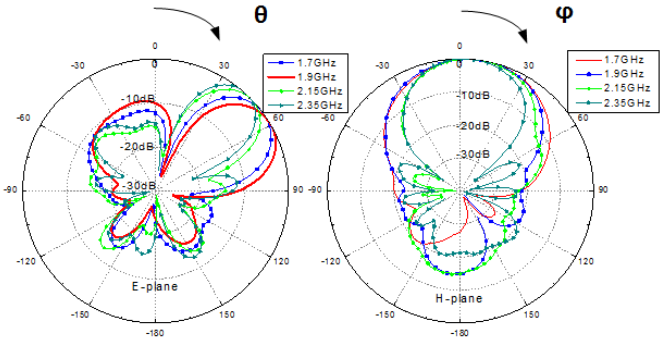


Fig. 20. Measured radiation patterns at the peak-gain frequencies.

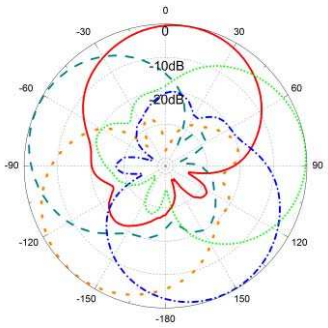


Fig. 21. Measured switched beams at 1.9 GHz in the H-plane.

degrades with frequency. On the other hand, the discrepancy between the measured and simulated results is caused by the model simplification in the simulation. To avoid generating large amounts of mesh cells in the cylindrical AFSS antenna structure, the thin substrate is omitted in the CST frequency domain simulation. So, the substrate loss leads to a lower measured gain. Other losses, such as conductor and diode losses, also contribute to the drop in the measured gain.

Radiation patterns were measured for several diode control voltages. Note that half of the AFSS cylinder (five columns) is biased while the other half is connected to zero bias voltage. It is expected that the same antenna performance will be realized if different half AFSS cylinders are selected owing to the structure symmetry. Fig. 20 shows the measured results in the E- and H-planes at the peak-gain frequencies. For most cases, there is good agreement between the simulation and measurement results. The higher level sidelobe and backlobe found in the two planes are the consequence of the imperfect

TABLE III

COMPARISON OF THE PROPOSED ANTENNA WITH PREVIOUS WORKS

| Ref No. | [12] | [13] | [16] | [26] | [30] | This work |
|---|---|---|---|---|---|---|
| Frequency tuning range | 54.5% | 46.4% | Dual band | 26.4% | No | 30% |
| Beam switching | No | No | Broadside | Broadside | Full azimuth | Full azimuth |
| Gain (dBi) | -1~6 | 0.21~1.2 | 5/5.4 | 5 | 8.7 | 7.4~10 |
| Dimensions | planar $0.7\lambda_0\times 0.7\lambda_0$ | planar $0.8\lambda_0\times 0.7\lambda_0$ | N/A | planar $0.7\lambda_0\times 0.7\lambda_0$ | $1.8\lambda_0\times 1.8\lambda_0\times 1.6\lambda_0$ | $1.4\lambda_0\times \lambda_0\times\lambda_0$ |

TABLE IV

POWER-CONSUMPTION COMPARISON

| Ref. No. | This work at 28.1V | This work at 15V | This work at 10.1V | This work at 7.5V | [16] | [30] |
|---|---|---|---|---|---|---|
| Power consumption | 27μW | 12.5μW | 6μW | 3μW | 182.4mW | 24mW |

replacement of the metallic reflector. It can be noted that for the E-plane radiation pattern at 1.7 GHz, the sidelobe is at −9.5 dB, which is higher than the simulated result. Fig. 21 shows the measured switched beam in the H-plane at 1.9 GHz. It is demonstrated that by successively selecting half of the AFSS cylinder, the generated beams are capable of covering the entire horizontal plane.

## V. DISCUSSION

Table III compares the characteristics of the previously reported works and our design described in Section III and Section IV. The work in this paper is capable of both frequency tuning and beam switching with a higher gain tuning range. Also, this is the first report of frequency and pattern reconfigurable antenna that can steer the beam covering 360° in the horizontal plane. Moreover, the maximum gain of the presented antenna is higher than any one of the cited papers in Table III, with a moderate frequency tuning range.

To provide insight into the antenna dc power rating, the power consumption of the proposed antenna at different tuning states is given in Table IV. Note that all the values are calculated when half of the AFSS cylinder is activated. The other half is not connected to the power supply so there is no power consumed. Also, the power consumption of the same slot AFSS structure (i.e., the same columns and rows as the configuration of this paper) loaded by p-i-n diodes is provided in Table IV. It is obvious that the varactor-loaded design features an extremely low power consumption: a level that is just 0.1% of that for the design employing p-i-n diodes [30].

## VI. CONCLUSION

The frequency tuning and beam switching characteristics of a novel antenna have been presented. A slot FSS array incorporating varactor diodes is employed to produce the passband tunability. When integrated with a feed antenna, the impedance matching and peak gain of the antenna can be tuned by varying the applied dc voltages. Directive beams

can be generated and swept in the horizontal plane by subtly reconfiguring a cylindrical FSS. The achieved 30% continuous tuning range results in a wider operation bandwidth than conventional FSS beam-switching antennas. Measured results show the realized gain varies from 7.4 to 10 dBi over the entire frequency tuning range. The antenna tuning bandwidth is limited by the varactor capacitance ratio, which determines the tuning range of the slot FSS. To the best of our knowledge, this is the first time a dc power consumption comparison has been undertaken for the beam-switching antenna applications using AFSS. The proposed antenna has a low cost and requires very low power to operate in its various states, and thus, it is a promising candidate for future wireless communication applications in which low cost and low power are required.

## ACKNOWLEDGMENT

The authors would like to thank S. Jakes from the University of Kent, Canterbury, U.K., D. Akins from Leonardo in the U.K., London, U.K., and the U.K. Royal Academy of Engineering (Industrial Secondment Scheme—ISS1617/48) for their support.

## REFERENCES

[1] W. A. Imbriale, S. Gao, and L. Boccia, *Space Antenna Handbook*. Hoboken, NJ, USA: Wiley, 2012.
[2] J. Costantine, Y. Tawk, S. E. Barbin, and C. G. Christodoulou, "Reconfigurable Antennas: Design and Applications," *Proc. IEEE*, vol. 103, no. 3, pp. 424–437, Mar. 2015.
[3] C. G. Christodoulou, Y. Tawk, S. A. Lane, and S. R. Erwin, "Reconfigurable antennas for wireless and space applications," *Proc. IEEE*, vol. 100, no. 7, pp. 2250–2261, Jul. 2012.
[4] S. Yang, C. Zhang, H. K. Pan, A. E. Fathy, and V. K. Nair, "Frequency-reconfigurable antennas for multiradio wireless platforms," *IEEE Microw. Mag.*, vol. 10, no. 1, pp. 66–83, Feb. 2009.
[5] J. T. Aberle, S. H. Oh, D. T. Auckland, and S. D. Rogers, "Reconfigurable antennas for portable wireless devices," *IEEE Antenna Propag. Mag.*, vol. 45, no. 6, pp. 148–154, Dec. 2003.
[6] R. L. Haupt and M. Lanagan, "Reconfigurable antennas," *IEEE Antennas Propag. Mag.*, vol. 55, no. 1, pp. 49–61, Feb. 2013.
[7] S. Genovesi, A. Di Candia, and A. Monorchio, "Compact and low profile frequency agile antenna for multistandard wireless communication systems," *IEEE Trans. Antennas Propag.*, vol. 62, no. 3, pp. 1019–1026, Mar. 2014.
[8] C.-Y.-S. Sim, T.-Y. Han, and Y.-J. Liao, "A frequency reconfigurable half annular ring slot antenna design," *IEEE Trans. Antennas Propag.*, vol. 62, no. 6, pp. 3428–3431, Jun. 2014.
[9] B. Liang, B. Sanz-Izquierdo, E. A. Parker, and J. C. Batchelor, "A frequency and polarization reconfigurable circularly polarized antenna using active EBG structure for satellite navigation," *IEEE Trans. Antennas Propag.*, vol. 63, no. 1, pp. 33–40, Jan. 2015.
[10] P. Bahramzy, O. Jagielski, S. Svendsen, and G. F. Pedersen, "Compact agile antenna concept utilizing reconfigurable front end for wireless communications," *IEEE Trans. Antennas Propag.*, vol. 62, no. 9, pp. 4554–4563, Sep. 2014.
[11] N. Behdad and K. Sarabandi, "Dual-band reconfigurable antenna with a very wide tunability range," *IEEE Trans. Antennas Propag.*, vol. 54, no. 2, pp. 409–416, Feb. 2006.
[12] S. V. Hum and H. Y. Xiong, "Analysis and design of a differentially-fed frequency agile microstrip patch antenna," *IEEE Trans. Antennas Propag.*, vol. 58, no. 10, pp. 3122–3130, Oct. 2010.
[13] A. Tariq and H. Ghafouri-Shiraz, "Frequency-reconfigurable monopole antennas," *IEEE Trans. Antennas Propag.*, vol. 60, no. 1, pp. 44–50, Jan. 2012.
[14] H. T. Liu, S. Gao, and T. H. Loh, "Electrically small and low cost smart antenna for wireless communication," *IEEE Trans. Antennas Propag.*, vol. 60, no. 3, pp. 1540–1549, Mar. 2012.
[15] C. Gu *et al.*, "Compact smart antenna with electronic beam-switching and reconfigurable polarizations," *IEEE Trans. Antennas Propag.*, vol. 63, no. 12, pp. 5325–5333, Dec. 2015.
[16] J. R. De Luis and F. De Flaviis, "Frequency agile switched beam antenna array system," *IEEE Trans. Antennas Propag.*, vol. 58, no. 10, pp. 3196–3204, Oct. 2010.
[17] G. Oliveri, D. H. Werner, and A. Massa, "Reconfigurable electromagnetics through metamaterials—A review," *Proc. IEEE*, vol. 103, no. 7, pp. 1034–1056, Jul. 2015.
[18] S. Lim, C. Caloz, and T. Itoh, "Metamaterial-based electronically controlled transmission-line structure as a novel leaky-wave antenna with tunable radiation angle and beamwidth," *IEEE Trans. Microw. Theory Techn.*, vol. 53, no. 1, pp. 161–173, Jan. 2005.
[19] H. Li *et al.*, "Reconfigurable diffractive antenna based on switchable electrically induced transparency," *IEEE Trans. Microw. Theory Techn.*, vol. 63, no. 3, pp. 925–936, Mar. 2015.
[20] J. C. Myers, P. Chahal, E. Rothwell, and L. Kempel, "A multilayered metamaterial-inspired miniaturized dynamically tunable antenna," *IEEE Trans. Antennas Propag.*, vol. 63, no. 4, pp. 1546–1553, Apr. 2015.
[21] W. Hu *et al.*, "Liquid crystal tunable mm wave frequency selective surface," *IEEE Microw. Wireless Compon. Lett.*, vol. 17, no. 9, pp. 667–669, Sep. 2007.
[22] F. Bayatpur and K. Sarabandi, "A tunable metamaterial frequency-selective surface with variable modes of operation," *IEEE Trans. Microw. Theory Techn.*, vol. 57, no. 6, pp. 1433–1438, Jun. 2009.
[23] B. Sanz-Izquierdo, E. A. Parker, and J. C. Batchelor, "Dual-band tunable screen using complementary split ring resonators," *IEEE Trans. Antennas Propag.*, vol. 58, no. 11, pp. 3761–3765, Nov. 2010.
[24] M. Safari, C. Shafai, and L. Shafai, "X-band tunable frequency selective surface using MEMS capacitive loads," *IEEE Trans. Antennas Propag.*, vol. 63, no. 3, pp. 1014–1021, Mar. 2015.
[25] D. Cure, T. M. Weller, and F. A. Miranda, "Study of a low-profile 2.4-GHz planar dipole antenna using a high-impedance surface with 1-D varactor tuning," *IEEE Trans. Antennas Propag.*, vol. 61, no. 2, pp. 506–515, Feb. 2013.
[26] F. Costa, A. Monorchio, S. Talarico, and F. M. Valeri, "An active high-impedance surface for low-profile tunable and steerable antennas," *IEEE Antennas Wireless Propag. Lett.*, vol. 7, pp. 676–680, 2008.
[27] M. N. Jazi and T. A. Denidni, "Agile radiation-pattern antenna based on active cylindrical frequency selective surfaces," *IEEE Antennas Wireless Propag. Lett.*, vol. 9, pp. 387–388, 2010.
[28] A. Edalati and T. A. Denidni, "High-gain reconfigurable sectoral antenna using an active cylindrical FSS structure," *IEEE Trans. Antennas Propag.*, vol. 59, no. 7, pp. 2464–2472, Jul. 2011.
[29] M. Niroo-Jazi and T. A. Denidni, "Electronically sweeping-beam antenna using a new cylindrical frequency-selective surface," *IEEE Trans. Antennas Propag.*, vol. 61, no. 2, pp. 666–676, Feb. 2013.
[30] B. Liang, B. Sanz-Izquierdo, E. A. Parker, and J. C. Batchelor, "Cylindrical slot FSS configuration for beam-switching applications," *IEEE Trans. Antennas Propag.*, vol. 63, no. 1, pp. 166–173, Jan. 2015.

**Chao Gu** received the B.S. and M.S. degrees from Xidian University, Xi'an, China, in 2009 and 2012, respectively, and the Ph.D. degree from the University of Kent, Canterbury, U.K., in 2017.

His current research interests include smart antennas and frequency selective surfaces.

**Steven (Shichang) Gao** (M'01–SM'16) is a Professor and Chair in RF and Microwave Engineering with the University of Kent, Canterbury, U.K.

**Benito Sanz-Izquierdo** is a Lecturer in electronic systems with the University of Kent, Canterbury, U.K.

**Edward A. Parker** is an Emeritus Professor of radio communications with the University of Kent, Canterbury, U.K.

**Wenting Li**, photograph and biography not available at the time of publication.

**Xuexia Yang**, photograph and biography not available at the time of publication.

**Zhiqun Cheng**, photograph and biography not available at the time of publication.